Continuous trench, pulsed laser ablation for micro-machining applications

G.B.J. Cadot[a], D.A. Axinte[a,*], J. Billingham[b]

[a]*Machining and Condition Monitoring Group, Faculty of Engineering, University of Nottingham, NG7 2RD, UK*
[b]*School of Mathematical Sciences, University of Nottingham, NG7 2RD, UK*

Abstract

The generation of controlled 3D micro-features by pulsed laser ablation in various materials requires an understanding of the material's temporal and energetic response to the laser beam. The key enabler of pulsed laser ablation for micro-machining is the prediction of the removal rate of the target material, thus allowing real-life machining to be simulated mathematically. Usually, the modelling of micro-machining by pulsed laser ablation is done using a pulse-by-pulse evaluation of the surface modification, which could lead to inaccuracies when pulses overlap.

To address these issues, a novel continuous evaluation of the surface modification that use trenches as a basic feature is presented in this paper. The work investigates the accuracy of this innovative continuous modelling framework for micro-machining tasks on several materials. The model is calibrated using a very limited number of trenches produced for a range of powers and feed speeds; it is then able to predict the change in topography with a size comparable to the laser beam spot that arises from essentially arbitrary toolpaths. The validity of the model has been proven by being able to predict the surface obtained from single trenches with constant feed speed, single

trenches with variable feed speed and overlapped trenches with constant feed speed for three different materials (graphite, polycrystalline diamond and a metal-matrix diamond CMX850) with low error. For the three materials tested, it is found that the average error in the model prediction for a single trench at constant feed speed is lower than 5 % and for overlapped trenches the error is always lower than 10 %. This innovative modelling framework opens avenues to: (i) generate in a repeatable and predictable manner any desired workpiece micro-topography; (ii) understand the pulsed laser ablation machining process, in respect of the geometry of the trench produced, therefore improving the geometry of the resulting parts; (iii) enable numerical optimisation for the beam path, thus supporting the development of accurate and flexible computer assisted machining software for pulsed laser ablation micro-machining applications.

Keywords: Pulsed Laser Ablation, Modelling, Micro-machining, Graphite, Diamond and related materials

2015 MSC: 00-01, 99-00

---

*Corresponding author

Email address: Dragos.Axinte@nottingham.ac.uk (D.A. Axinte)

Nomenclature

(x, y, z)	Coordinate system, c.f. Figure 1	P	Laser Power
		$p(y, P, v_{\text{feed}})$	Trench profile
t	Time	$\bar{p}$	Generic Profile
$\underline{x}$	Vector position of the point (x, y)	E	Ablation Rate
$\underline{x}_{\text{path}}(t)$	Vector of the beam path equal to $(x_{\text{path}}(t), y_{\text{path}}(t))$	$\bar{E}(P, v_{\text{feed}}, r)$	Generic Ablation Rate
		$\alpha(P)$	Function of the trench depth variation the feed speed
$v_{\text{feed}}(t)$	Feed speed $\lvert\partial_t \underline{x}_{\text{path}}\rvert$		
s_{path}	Arc length of the beam path	$\beta(P)$	Function of the trench depth variation inter-pulses interactions
r	Distance from the centre of the beam $\underline{x}_{\text{path}}$ to the point $\underline{x}$		
Z	Depth of the surface at the point of coordinate (x, y)	$r^*(P)$	Function of the width of the trench

1. Introduction

With its capability to generate small features, pulsed laser ablation (PLA) offers new possibilities for microprocessing/structuring of a large variety of difficult-to-cut materials such as, high strength Ti/Ni based superalloys (e.g. Ti6Al4V [1], Inconel 718 [2]), ceramics (e.g. SiC [3], Al_2O_3 [4]) and super-hard materials (e.g. diamond [5], cubic boron nitride [6]). This, in conjunction with the decrease in capital cost for high power lasers, makes pulsed laser ablation a viable machining method for high value-added industries (e.g. medical, aerospace, defence, microelectromechanical systems). PLA has the capability to machine parts with complex geometries (e.g. cutting

insets [7], dressing/truing tools [8], micro-grinding wheels [9], ink-jet holes [10], etc.) for which conventional (turning, grinding and milling) and other non-conventional (e.g. abrasive water jet, electrical discharge) machining processes might not be appropriate due to the small size of the feature to be generated or limitations caused by the hardness/strength of the workpiece material or other part quality related issues (e.g. heat affected zones).

Although PLA has some significant advantages in micro-machining, it also faces some major challenges: (i) apart from the beam characteristics (pulse energy, temporal profile of the pulse and spatial profile of the pulse) and kinematic parameters (vector of propagation of the beam and feed velocity), it is a time dependent process; the accelerations and decelerations caused by the machine stages/optics (i.e. galvanometric mirrors) dynamics result in non-uniformity of the ablation process, thus leading to inherent variation of the machining quality; (ii) because PLA occurs in a small area (spot size < 50 µm) [11] and a short time (<200 ns) [12] while generating molten debris and noise (e.g. plasma emission, electron generation etc.) [13, 14], the process is difficult to monitored online; (iii) the material removal mechanisms are diverse and complex as they depend on the wavelength and temporal profile of the laser pulse; furthermore some removal mechanisms (i.e. explosive boiling, homogeneous vaporization, etc.) are not entirely understood [15, 16]. Thus, not surprisingly, PLA has been a significant research subject for micro-machining in the last two decades.

Despite the ever-increasing use of lasers for micro-machining, it very often requires lengthy and costly experimental studies to estimate the optimum beam path and process parameters for the generation of specific micro-

features [17]. The development of a beam path strategy is not a trivial task for freeform structures and normally involves a number of iterations, with measurements being done on the resulting part at each iteration to enable the optimisation of the process parameters and beam path. This can be a barrier for some potential users of laser machining, especially those who need to create innovative freeform structures.

In this context, the avoidance of a "trial and error" experimental approach requires the development of a computationally inexpensive mathematical model for PLA, which will enable a step-change in the process control. However, little attention has been given to this issue and there are few examples in the literature on modelling of PLA for large scale machining tests. Nevertheless, attention has been given to the development of physical models, which study the fundamental interaction between the laser beam and the material.

The development of physical models to describe the conservation of heat, mass and momentum, using the finite difference/element/volume methods to solve the system of equations, requires HPC computational power to calculate the three dimensional solution in a realistic period [18]. Therefore, most of the models presented in the literature are one [15] or two [19] dimensional systems of equations; hence, not covering the full 3D information needed for the simulation of freeforms to be generated by PLA. These models have mainly been developed to provide useful insight into the phenomena occurring during pulsed laser ablation for the interaction of a single or low number of pulses with the target surface. However, following this approach, the simulation of one laser pulse interacting with the target requires several minutes

with a standard computer. As the simulation of a surface generated by PLA can require tens of thousands of pulses, this would last at least several days. Thus, physical modelling of PLA cannot be applied for optimisation of the beam path and process parameters for micro-machining of complex geometry surfaces.

Recently, more consideration has been given to computationally inexpensive approaches [6]. Those methods, unlike the physical models, focus on estimation of the footprint of PLA as a function of the variable parameters during the machining process, see Figure 1. These approaches encompass modelling (i) based upon simplified assumptions such as rectangular temporal profile of the laser pulse [19], constant material properties over a large temperature range [20], material removal over a defined temperature/energy [21] which does not provide good accuracy for the profile of the trench and might still require significant computing power; (ii) based on artificial intelligence methods (neural network, genetic algorithms, etc.)[22, 23, 24], that require a significant set of data for training the algorithm, are not able to capture the details of the physics of the process, work only within the range in which they have been trained and cannot be modified to capture experimental observation of overlapped pulses; (iii) based on empirical calibration [1, 25, 26] that describe the interaction between the workpiece and one pulse from the laser by fitting the result from experimental data; the main drawback of this method is the loss of accuracy during overlapping of pulses [25, 26].

From these families of modelling frameworks, the model that relies on empirical calibration seems to be the one that gives better results and high ver-

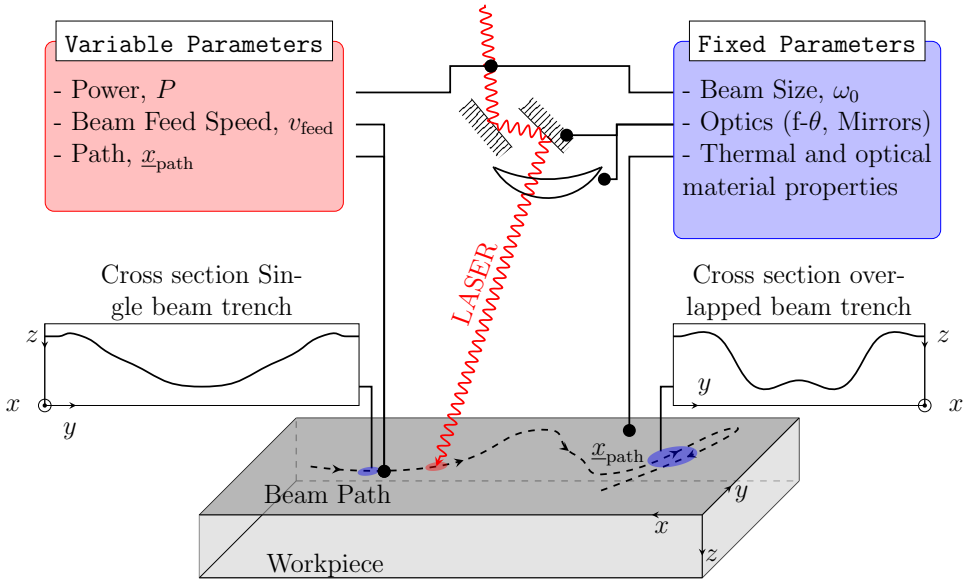

Figure 1: Variable and fixed parameters used in the model for PLA machining.

satility; however it cannot accurately simulate large scale machining [25, 26]. Usually, empirical calibration modelling has been developed considering the interaction between laser and target on a pulse-by-pulse evaluation of the laser ablation process [1, 24, 26]. This approach has difficulties in accounting for the interaction between two consecutive pulses such as preheating [18, 27], surface property modification [28], material ejection [18] that are present during nanosecond ablation with a high level of overlapping and rapid repetition rate of the pulses. Generally, a high level of overlapping of the pulses is used to obtain a machined surface with a low roughness; therefore, the pulse-to-pulse description is not the best method to predict accurately the workpiece micro-topography in real-life machining [25, 26].

In order to address these drawbacks, this paper presents an innovative model in which the ablation of the surface by the pulsed laser is treated as a

continuous process, so that the interaction between two pulses is implicitly taken into account in the values of the calibrated parameters. Unlike, previous modelling approaches, the framework enables the modelling of non-linear interaction between pulses. It also requires little experimental data for an accurate calibration of the model and opens the way for continuous optimisation of the machining parameters to generate a specific topography. The model does not have any inherent restriction on the material or lasers used and can easily be calibrated with a few experimental tests. This model for micro-machining takes into consideration the following aspects:

- Beam feed speed: the variation of the trench depth with the degree of overlapping of the pulses. This takes into account heat conservation between pulses, material ejection and surface property modification.
- Position of the beam on the surface: allowing the prediction of the 3D surface resulting from the machining process.
- Beam Power: the variation of the width and depth of the trench with the power.

The modelling approach is validated for three materials (POCO graphite AF-5, metal-matrix diamond CMX850 and a polycrystalline diamond, PCD) as an example of its accuracy, for both single and overlapped trenches, thus making the first step towards controlled and predictable micro-machining by PLA of truly complex geometries.

2. Modelling of continuous trench PLA for an arbitrary moving beam

This section provides the mathematical framework used to model the interaction between the laser beam and the workpiece.

2.1. Model of a single footprint of an arbitrary moving beam

The variation in the depth, Z, at the point $\underline{x} = (x, y)$, due to the impact of the laser beam moving on the tool path, $\underline{x}_{\text{path}} = (x_{\text{path}}, y_{\text{path}})$, is expressed by a general relation,

$$\frac{\partial Z}{\partial t} = E\left(P, v_{\text{feed}}, \sqrt{(x - x_{\text{path}})^2 + (y - y_{\text{path}})^2}\right). \tag{1}$$

The ablation rate, E, is calculated from experimental data. The following calculation shows that the ablation rate can be expressed using the profile of a trench, $p(y, P, v_{\text{feed}})$. From experiments presented in the paper, it has been found that the profile of a trench at constant feed speed, v_{feed}, and power, P, can be expressed as

$$p(y, P, v_{\text{feed}}) = \left[\frac{\alpha(P)}{v_{\text{feed}}} + \beta(P)\right] \bar{p}\left(\frac{y}{r^*(P)}\right), \tag{2}$$

with α(P) the factor for the variation of the depth with the inverse of the feed speed, β(P) the factor for the effect of the pulse interaction on the profile depth, r^* the width of the trench profile (that is not directly related to the spot size), y the position across the profile of the trench and $\bar{p}$ the generic profile of the trench. Using the notation r as the distance between the centre of the beam, $\underline{x}_{\text{path}}$, and a point on the surface, $\underline{x}$, it is possible to express

the depth, Z, as a function of the ablation rate assuming that $Z(x, y, t) = 0$ when $t = 0$ (for the demonstration, see Appendix A), as

$$Z(x, y, P, v_{\text{feed}}) = \int_{s_{\text{start}}}^{s_{\text{end}}} \frac{E\left(P, v_{\text{feed}}, r\right)}{v_{\text{feed}}} \mathrm{d}s_{\text{path}}. \tag{3}$$

where s_{path} is the beam path arc length. Since the ablation rate, E, has a compact support and the beam is moving with a constant feed speed in the x direction, it is possible to simplify this equation as the depth does not depend on x to give (for the demonstration, see Appendix A)

$$v_{\text{feed}}\ Z(y, P, v_{\text{feed}}) = \int_{-\infty}^{\infty} E\left(P, v_{\text{feed}}, r\right) \mathrm{d}x_{\text{path}}. \tag{4}$$

Assuming that the beam path is centred on the y axis, it gives,

$$\mathrm{d}x_{\text{path}} = \frac{r\mathrm{d}r}{\sqrt{r^2 - (y - y_{\text{path}})^2}}, \tag{5}$$

and using the Abel transform [29], the ablation rate is,

$$E(P, v_{\text{feed}}, r) = -\frac{v_{\text{feed}}}{2\pi} \int_{r}^{\infty} \frac{\partial_y p(y, P, v_{\text{feed}})}{\sqrt{y^2 - r^2}} \mathrm{d}y. \tag{6}$$

Using Equation (2), the ablation rate, E, is equal to,

$$E(P, v_{\text{feed}}, r) = \left[\frac{\alpha(P) + \beta(P) v_{\text{feed}}}{r^*(P)}\right] \left[-\frac{1}{2\pi} \int_{\bar{r}}^{\infty} \frac{\partial_{\bar{y}} \bar{p}\left(\bar{y}\right)}{\sqrt{\bar{y}^2 - \bar{r}^2}} \mathrm{d}\bar{y}\right], \tag{7}$$

with,

$$\bar{y} = \frac{y}{r^*(P)} \text{ and } \bar{r} = \frac{r}{r^*(P)}, \tag{8}$$

with $\bar{r}$ the radial distance normed with respect to the width of the trench. Equation (7) can be rewritten as:

$$E(P, v_{\text{feed}}, r) = \left[\frac{\alpha(P) + \beta(P) v_{\text{feed}}}{r^*(P)}\right] \bar{E}(\bar{r}), \tag{9}$$

with the generic ablation rate, $\bar{E}$, only dependent on the generic profile, $\bar{p}$,

$$\bar{E}(\bar{r}) = -\frac{1}{2\pi} \int_{\bar{r}}^{\infty} \frac{\partial_{\bar{y}} \bar{p}\,(\bar{y})}{\sqrt{\bar{y}^2 - \bar{r}^2}} \mathrm{d}\bar{y}. \tag{10}$$

Equation (9) is particularly interesting. It shows that the ablation rate can be expressed using two factors. The first factor represents the variation of the ablation rate with the power and feed speed of the beam. The second factor, $\bar{E}(\bar{r})$, represents the constant shape of the material removal rate. This separation makes it possible to isolate the influence of each parameter and therefore, calibrate each part of the ablation rate separately.

2.2. Calibration of the model

The ablation rate presented above, Equation (9), needs to be calibrated. A simple method to calibrate the ablation rate is to produce a series of trenches over a range of feed speed (i.e. overlapped pulses) and power; this requires a large data set of profiles to calibrate each function accurately. To ease the constraint on the amount of experimental data required to correctly calibrate the model, a new calibration method has been developed that

greatly reduces the amount of experimental data necessary.

The mathematical justification for this new method is given in Appendix B. It demonstrates that a particular variation of the feed speed results in a surface that contains all the information necessary for the calibration of the parameters for a given power of the laser beam. The profile of the trench for a particular x and y is directly related to α, β and the feed speed of the beam through

$$p(x, y) = \left[\frac{\alpha}{v_{\text{feed}}(x)} + \beta\right] \bar{p}(\bar{y}). \tag{11}$$

Therefore, it greatly reduces the number of trenches needed for an accurate calibration of the model.

3. Methodology

The model described above ultimately needs to be integrated into laser machining CAD/CAM systems. Consequently, the agreement of the model only with single trenches is not a full test of its use in machining environments, for which a feed speed variation and the overlapping of trenches is fundamental to the manufacturing of 2.5D/3D freeform parts. Thus, additional tests have been conducted to characterise the performance of the model in the following distinct conditions: (i) arbitrary moving beam, (ii) overlapped trenches. The two sets of tests are not real-life machining tests but are arguably closer to real machining conditions for generating freeforms. They have been chosen for the simplicity of their implementation but mostly because it is possible to precisely monitor the process, accurately calculate the error and find possible deficiencies from the modelling perspective. In this

paper, many conditions for constant feed speed single trenches are tested for the three materials. Afterwards, tests for a reduced number of cases with a feed speed variation and overlapping trenches are performed to demonstrate that the model is accurate for a large set of kinematic conditions. Thus, the combination of the two sets of tests offers a comprehensive view of the model's capabilities.

The methodology for the calibration and the validation of the model consists of the following steps.

Step 1, Calibration: generate a series of trenches for a range of feed speeds and powers. The resulting trenches are measured using a white light interferometer (WLI); then, the depth at the centre of the trench and profiles of the trench are extracted and used to calibrate the model as per the work-flow presented in Figure 2.

Step 2, Validation and error quantification for the proposed model for constant feed speed single trench. A series of trenches with constant feed speed and power are produced and then measured. Afterwards, the cross-section (2D) of the surface (3D) is calculated by averaging the profile along the beam path over at least 150 µm. Then, the cross-sections are compared with simulations and the errors are evaluated.

Step 3, Evaluation of the model error for a single trench with a continuous feed speed variation. A series of trenches for a range of powers and varied feed speed is produced for each material. The depth at the centre of the trench is extracted from the experimental set and compared to the numerical one.

Step 4, Evaluation of the model for overlapped trenches. The feed speed and power are kept constant for both trenches and the distance between the

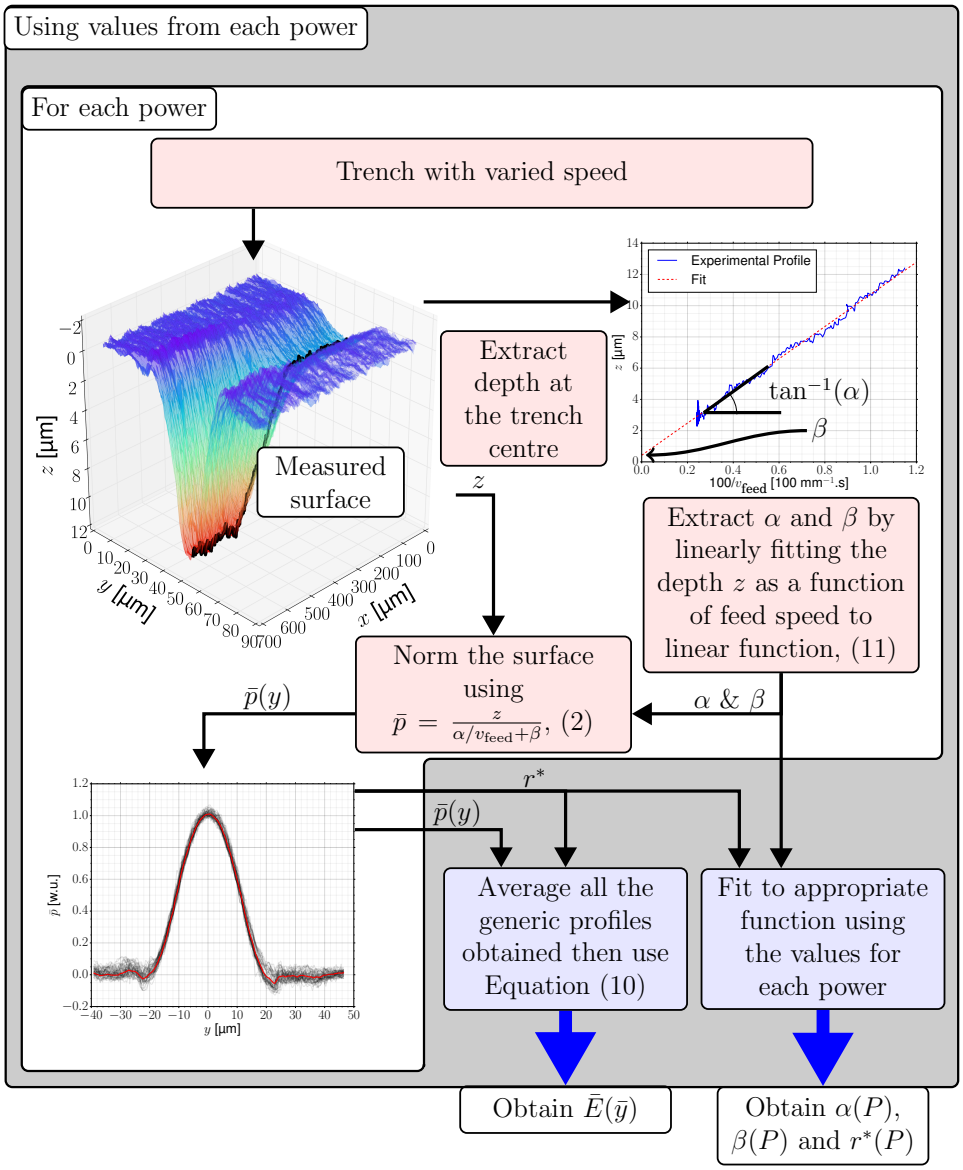

Figure 2: Diagram of the calibration work-flow, the plot presented are an example of the calibration process for CMX850 at 8.07 W.

centres of the two trenches (i.e. step-over) is varied. The cross-sections (by averaging the profile over 150 µm) extracted from the surfaces are analysed, compared with the simulations and the errors are calculated.

The errors have been evaluated as the relative error of the area of the simulated cross section compared to the experimental value. One should bear in mind that, even if the feed speed is kept constant, there is variability in the material removal process along the trenches due to several factors: (i) variation of the pulse to pulse energy (ca. 5%); (ii) the feed speed variation along the path (ca. 3%); (iii) distribution of side-effect/surface defects (e.g. graphitic material for mechanical PCD, tungsten and cobalt for CMX850 and void distribution for graphite); (iv) errors in the flatness of the initial surface and roughness variation. Thus, the evaluation of the errors must be interpreted with caution because it is believed that a significant part of the error could be associated with the above-mentioned variabilities.

4. Experimental setup and measurement methods

The experimental tests for the model validation are conducted with a SPI-G3 HM fiber laser utilising a constant pulse repetition rate of 35 kHz. Its temporal profile is characterised by a full–width at half–maximum of 30 ns with a long trail after the maximum that lasts approximately 200 ns. The spatial profile of the laser pulse outside the laser head is an elliptic Gaussian characterised by a width of 2.1mm (using the $1/e^2$ definition) and an ellipticity of 0.851. The beam is directly fed into the galvanometer head; an f-θ lens, of 100 mm focal length, is used to focus the beam onto the workpiece. The resulting spatial profile is a beam width of around 45 µm (using the $1/e^2$ definition) with an ellipticity of 0.956 at the focal plane. The power measured at the focal plane can be varied from 0W to 18.8W. For all the experimental trials, a custom Aerotech system with a 2D Galvanometer head

to control the laser beam positioning and a 4 axis stage for the sample positioning are used. The setup is designed for high precision micro-machining, as the galvanometer offers an accuracy of 1 µm over the whole field of view. The sample positioning stage also offers 1 µm accuracy in the focal plane. To avoid distortion of the laser beam spot due to the angle introduced by the f-θ lens, the tests are carried out in the 1 mm square at the centre of the field of view.

The resulting surface is measured using a white light interferometer, Bruker GT-i, with a pixel size of 197 nm to reduce the measurement error due to the small size of the feature ($<$ 30 µm) and the high slope of the surface (can be as high as 70°).

For the purpose of validating the modelling framework, the model is calibrated and tested on three materials. The first material is an isotropic graphite, POCO AF-5, exhibiting small grain size of 1 µm and a void quantity of 20%. This material presents low recast material at the rim of the trench making it a good candidate for the validation of the modelling approach. The second material is a metal-diamond composite CMX850, with high wear resistance and strength due to the small diamond grain size and is widely used in micro-tooling [11]. CMX850 has a diamond grain ($<$10 µm) in a metal matrix of tungsten and cobalt. The last material is a CVD mechanical grade polycrystalline diamond (referred as mechanical PCD) used for manufacturing insets for turning [30] or for micro-tooling [31]. This material has a large grain size with graphitic phase present at the grain boundaries.

In order to avoid noise in the PLA trenches to enable accurate validation of the model, a smooth initial target surface is needed, so the roughness of the

samples has been reduced by polishing if possible. For the graphite POCO AF-5, the samples have been manually polished; an R_a value of 50 nm has been achieved. In the case of CMX850 and mechanical PCD, the samples could not be manually polished due to the hardness of the materials; an R_a of 200 nm has been observed for these samples.

5. Results and discussion

The first subsection presents the calibration process step by step using the graphite POCO AF-5 as an example. Each step of the calibration is critically evaluated and the possible errors discussed. Then, the model errors for each test are evaluated for the three materials and discussed in detail. Several examples of the machined surface are presented. The error tables offer a comprehensive view of the ability of the model to predict the resulting topography of PLA micro-machining.

5.1. The calibration method: example of graphite POCO AF-5

Calibration of the model requires a series of trenches with a specific feed speed variation along the trench at different levels of power. The resulting trenches are scanned and then the depth at the centre of the trench is extracted, see Figure 3(a). As demonstrated in Appendix B, the depth measured at a certain position along the axis x, see Figure 1, is equal to the depth that a single trench at a constant feed speed will produce for a given power. The parameters α and β of the linear fit are extracted by matching the depth and the feed speed using Equation (11), see Figure 3(b). This process is challenging because the depth at the centre of the trench exhibits

variation due to the errors of the process (as discussed in subsection 3); this is especially visible at constant feed speed when the depth at the centre of the trench has a near constant depth, see Figure 3(a). It should be noted that an error of 10-20µm in the positioning of the feed speed profile compared to the depth profile can introduce uncertainties of up to 5% in the value of linear fit. Once the positions of the two profiles are correctly aligned, it is possible to extract the values of α and β at a particular power level, see Figure 3(b).

The calibration process can be repeated for as many power levels as necessary over the range studied; for graphite POCO AF-5, 8 different powers were used to calibrate α, β and r^*. The values of α and β as a function of the power are shown in Figure 4(b), 4(c). The next parameter to calibrate is the variation of the width of the profile, r^*, with respect to the power, see Equation (9). It is possible to extract the generic profile, $\bar{p}(y)$, of the trench once α and β have been calibrated. The surface, shown in Figure 5, is obtained by

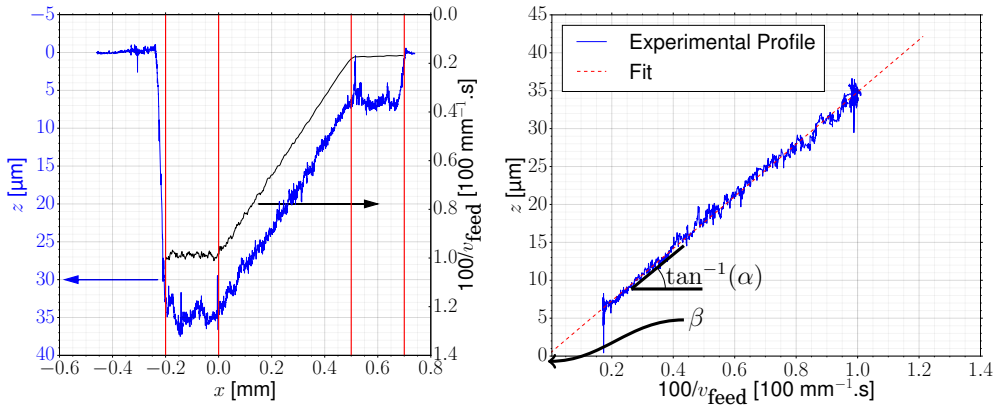

Figure 3: Calibration for graphite POCO AF-5 at 10.24 W; (a) Extracted profile along the trench, (b) fit of the depth as a function of the inverse of the feed speed by a linear function.

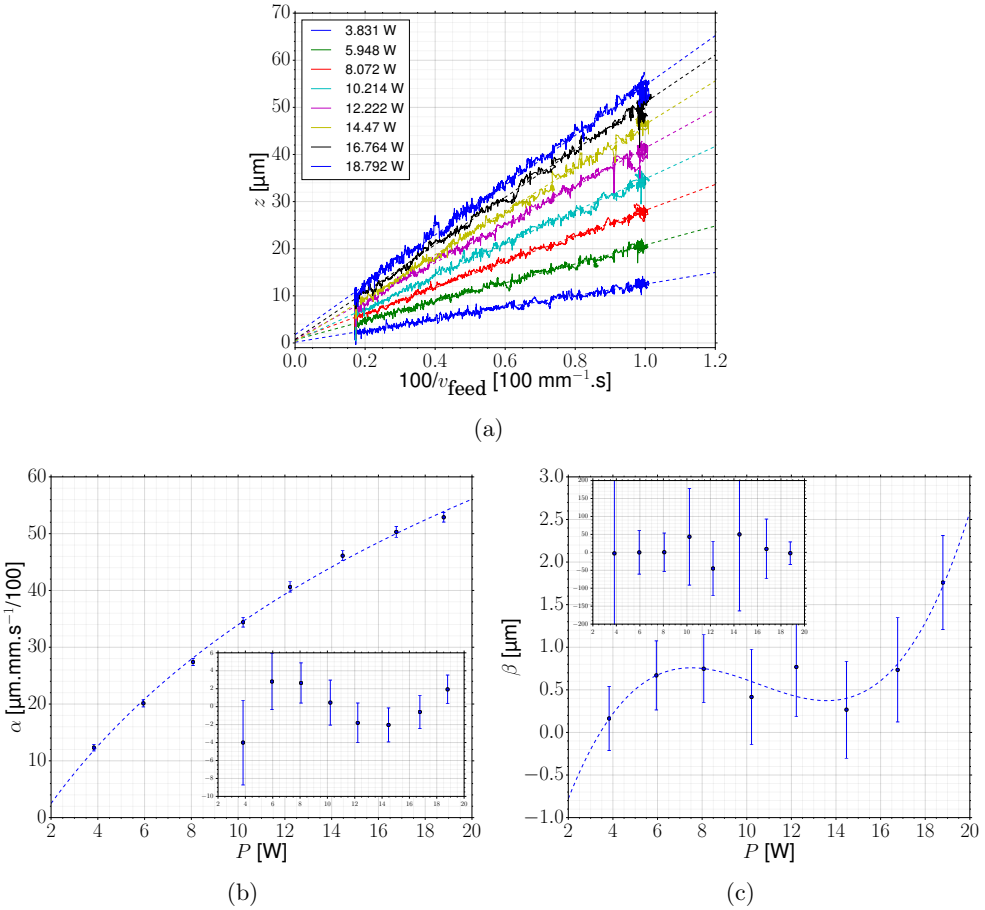

(a)

(b)

(c)

Figure 4: (a), extracted profile along the trench for a range of power used in the calibration; (b), fit for α (the inset is the relative error of the fit in percentage); (c), fit for β (the inset is the relative error of the fit in percentage).

normalising the depth of the trench along the path by $\alpha/v_{\text{feed}}(x) + \beta$ using Equation (11). It is apparent from Figure 5 that the calibration has been done correctly since the value at the bottom of the profile along the trench is close to 1. The generic profile of the trench for this power is extracted by averaging the profiles along the path. This process is repeated for each power level.

The characteristic width of the profile, r^*, is obtained by measuring the

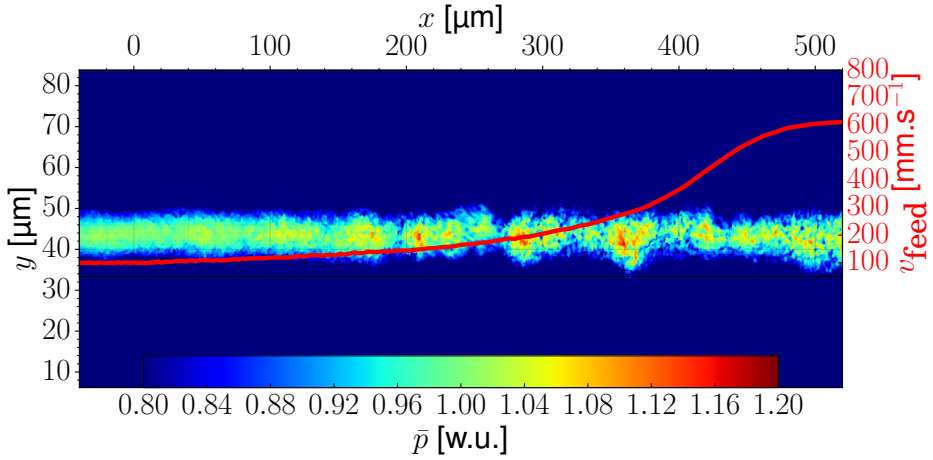

Figure 5: Normalised surface using α and β, see Figure 4 at 14.47 W on Graphite POCO AF-5.

distance from the centre of the profile to the position such that the value of the depth is less than 20% of the maximum depth. This threshold is chosen as a good trade-off between the noise caused by the initial surface roughness of the part and acceptable measurement accuracy of the generic profile width.

In Figure 6(a), the width of the profile as a function of the power is presented. The profile extracted from the normalised surface, Figure 5, is presented in 6(b). It is clear that the shape of the generic profiles of the trenches for all powers and feed speeds are close and justifies the assumptions made in Equation (2) for the modelling of the PLA. The most striking observation to emerge from the Figure 6(b) is that, with the ranges of the tested parameters, the ablation rate does not depend on the slope of the profile. One might expect that the slope highly affects the ablation on the side of the profile due to the increased surface of interaction leading to a reduction of the fluence. It is not the case for the ablation of trenches of the

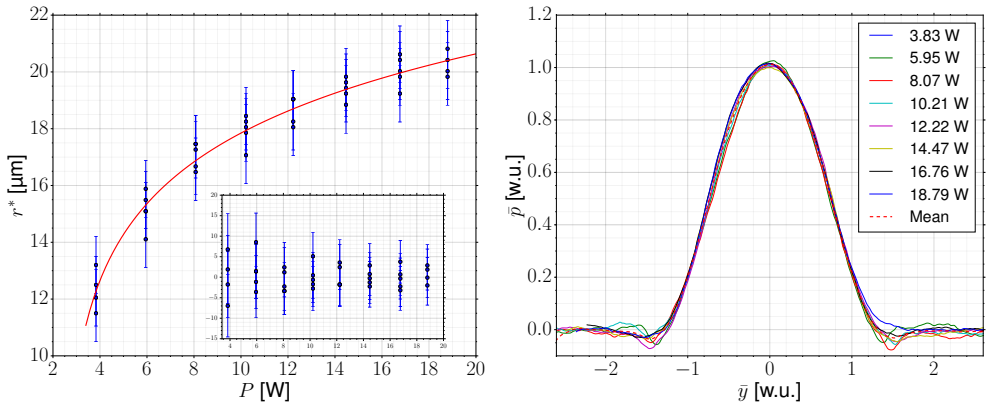

(a) (b)

Figure 6: (a), Fit for r^* (the inset is the relative error of the fit in percentage); (b), generic profiles of the trench for all the powers used in the calibration.

materials studied (graphite POCO AF-5, CMX850 and mechanical PCD), at least for a slope of the side of the trench lower than 75 °.

The simulation of the machining process for a laser beam requires the calculation of the generic ablation rate; this relates to Equation (1) and Equation (9). Knowing the generic profile, it is possible to obtain the generic ablation rate using Equation (10). A numerical inverse Abel transform [32] is used to calculate the generic ablation rate from the mean of the generic profile presented in Figure 6(b). The generic ablation rate, for graphite POCO AF-5, is presented in the Figure 7.

For graphite POCO-AF5, the model has been calibrated for a range of powers [4, 18.8] W and a range of beam feed speeds [100, 600] mm.s^{-1}. The model has also been calibrated for CMX850 and mechanical PCD for the power in a range of respectively [6, 18.8] W and [8, 18.8] W, for the beam feed speed in a range of respectively [100, 400] mm.s^{-1} and [100, 300] mm.s^{-1}.

The maximum range of calibration depends on the material properties

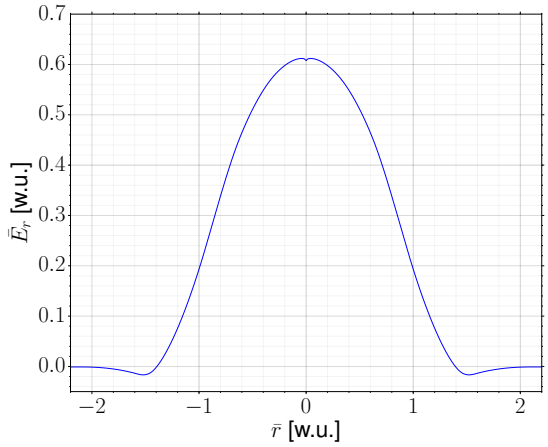

Figure 7: The normalised ablation rate $\bar{E}$ for the Graphite POCO AF-5.

and is determined by two criteria: (i) the feed speed cannot exceed a critical value for which separate pulses are observable; hence, not obtaining a trench (such that the bottom of the trench has a constant depth); (ii) a low feed speed generates a large amount of debris and thermal damage to the surface/target and should be avoided, furthermore the slope of the trench ($>$ 70°) and depth are too large for the measurement system used thus prone to measurement errors; (iii) the lower limit of the power is the ablation threshold of the material. Thus, the model is aimed at the generation of acceptable micro-machining surfaces.

5.2. Single trenches with constant direction and beam feed speed

The error calculations are made using the method described in section 3. For graphite, CMX850 and mechanical PCD, the error tables are respectively presented in Table 1, 2 and 3. The maximum (Δ_{Max}) and average (Δ_{Avg}) errors are: Δ_{Max}=10% and Δ_{Avg}=4.11% for graphite, Δ_{Max}=8% and

Table 1: Relative error in the area of the trench cross section for the Graphite POCO AF-5 for single trenches with a constant direction and value of the beam feed speed

		Power [W]										
		2.6	3.77	5.04	6.27	7.45	8.62	9.85	11.1	12.02	15.95	17.97
		Relative Error [%]										
Feed Speed [mm.s^{-1}]	150	3.71	2.56	7.12	5.16	5.06	6.00	4.06	8.13	8.29	9.12	9.65
	200	2.38	2.01	0.60	7.22	5.20	6.43	5.41	2.95	1.29	1.23	1.88
	300	2.35	1.89	3.36	1.20	1.11	2.24	1.38	1.18	1.49	4.23	3.38
	400	3.27	6.52	1.85	6.72	4.49	6.69	9.81	7.17	6.87	7.78	1.97
	500	6.77	2.28	3.49	2.58	3.69	1.48	1.14	1.40	1.78	3.41	4.95
	600	—	7.85	2.22	2.26	1.53	1.82	2.05	1.05	3.84	2.81	7.35
	700	—	7.67	2.90	4.03	6.45	8.24	4.07	3.91	4.99	4.45	8.41

Δ_{Avg}=3.69% for CMX850 and Δ_{Max}=7% and Δ_{Avg}=4.81% for mechanical PCD.

For the three target materials studied, the error values are scattered from 10% to less than 1% without revealing any evident pattern which suggests that their origin is variability in the process. Average error values for each material are lower than 5% giving a good indication that the model is in good agreement with the experimental results. Studying in detail the performance of the model for single trenches is key to ensuring the consistency of the following tests that show the performance of the modelling framework for real machining tests.

5.3. Single trenches with constant direction and variable beam feed speed

The feed speed variation during laser machining affects the removal rate, therefore controlling the depth of the profile. To compare the model and

Table 2: Relative error in the area of the trench cross section for CMX850 for singles trenches with a constant direction and value of the beam feed speed

		Power [W]						
		5.95	8.07	10.12	12.22	14.47	16.76	18.79
		Relative Error [%]						
Feed Speed [mm.s^{-1}]	100	4.70	5.46	7.81	5.91	3.62	3.00	2.18
	150	3.82	2.98	1.27	1.49	3.45	3.02	1.79
	200	7.28	1.97	1.04	3.64	1.22	1.38	7.37
	300	2.28	1.23	2.37	5.18	2.64	1.69	8.69
	400	4.60	1.92	6.5	2.82	5.32	2.21	3.54

experimental results, the depth at the centres of the profiles along the path are shown in Figure 8.

It is apparent from Figure 8 that the model is in excellent agreement with experimental tests for the three workpiece materials. The model does not take into account the variability of the process and therefore it predicts the local average depth that will be found without the roughness. Interestingly, the experimental depths present some larger scale (depth $\geq$ 500 nm and length $\geq$ 100 µm) fluctuations along the trench. This suggests that the error variations, presented in Tables 1, 2 and 3, might come from intrinsic variability of the process parameters and macro-micro geometry of the initial workpiece surfaces.

Table 3: Relative error in the area of the trench cross section for Mechanical PCD for single trenches with a constant direction and value of the beam feed speed

		Power [W]					
		8.07	10.12	12.22	14.47	16.76	18.79
		Relative Error [%]					
Feed Speed [mm.s^{-1}]	100	3.21	1.93	3.8	5.02	4.30	3.23
	128	5.89	5.60	5.49	6.07	3.39	4.13
	200	4.85	3.58	3.02	4.94	4.37	3.39
	300	—	3.5	2.71	2.46	1.87	1.55

5.4. Overlapped trenches with constant direction and beam feed speed

Experiments to validate the model for overlapped trenches at normal beam incidence were carried out for several powers and feed speeds by varying the distance between the centre of the two trenches from 0 µm to a maximum of 60 µm while keeping feed speed and power constant. In Figure 9, four tests on CMX850 are presented at 14.47 W and 300 mm.s^{-1}.

The relative errors between the model and the experimental results are presented in Table 4. The model accurately predicts the results of overlapping trenches for graphite POCO AF-5, CMX850 and mechanical PCD. The results are particularly good for graphite POCO AF-5 and CMX850, with an error usually less than 5%.

In the case of the mechanical PCD, the errors increase for high level over-

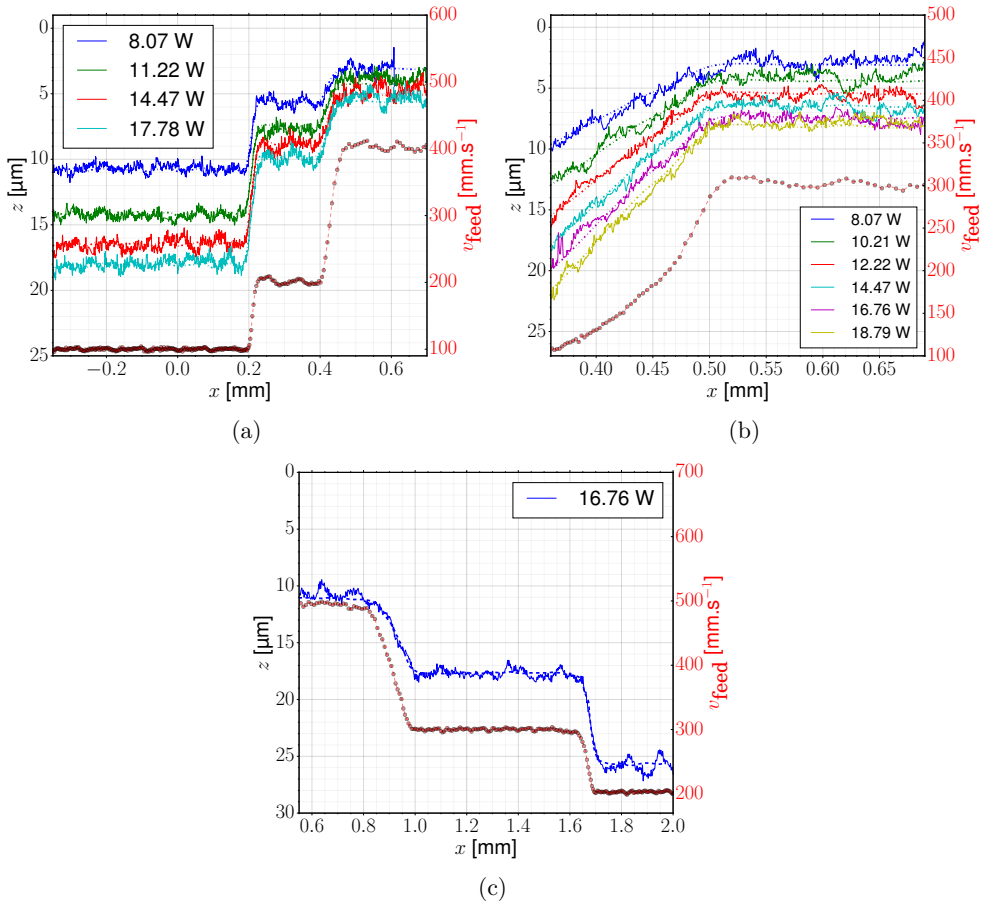

Figure 8: Feed speed variation tests for (a) CMX850, (b) Mechanical PCD and (c) graphite POCO AF-5. Solid line (-) experimental depth, dashed line (- -) simulation and red (-○-) measured feed speed.

lapping (overstep ≤ 30 µm). This might be caused by variability of the laser operating parameters or inaccuracies in the measurement of the surfaces, but it is likely that a great part of them is related to non-linear effects that are not presently taken into account by the model. In this respect, it should be noted that for mechanical PCD, the absorption of the laser relies mainly on the presence of impurities, such as amorphous carbon, which exists between the diamond grains [33]. In effect, the absorption coefficient of pure diamond

is lower than 1 m^{-1} whereas the graphite absorption coefficient is around 10^8 m^{-1}. Previous studies of pulsed laser ablation of diamond [28, 34] have shown that diamond ablation is always accompanied by the transformation of a diamond layer into graphite. Hence, diamond is metastable at ambient pressure and temperature; above 2000 °C diamond is transformed into graphite [35].

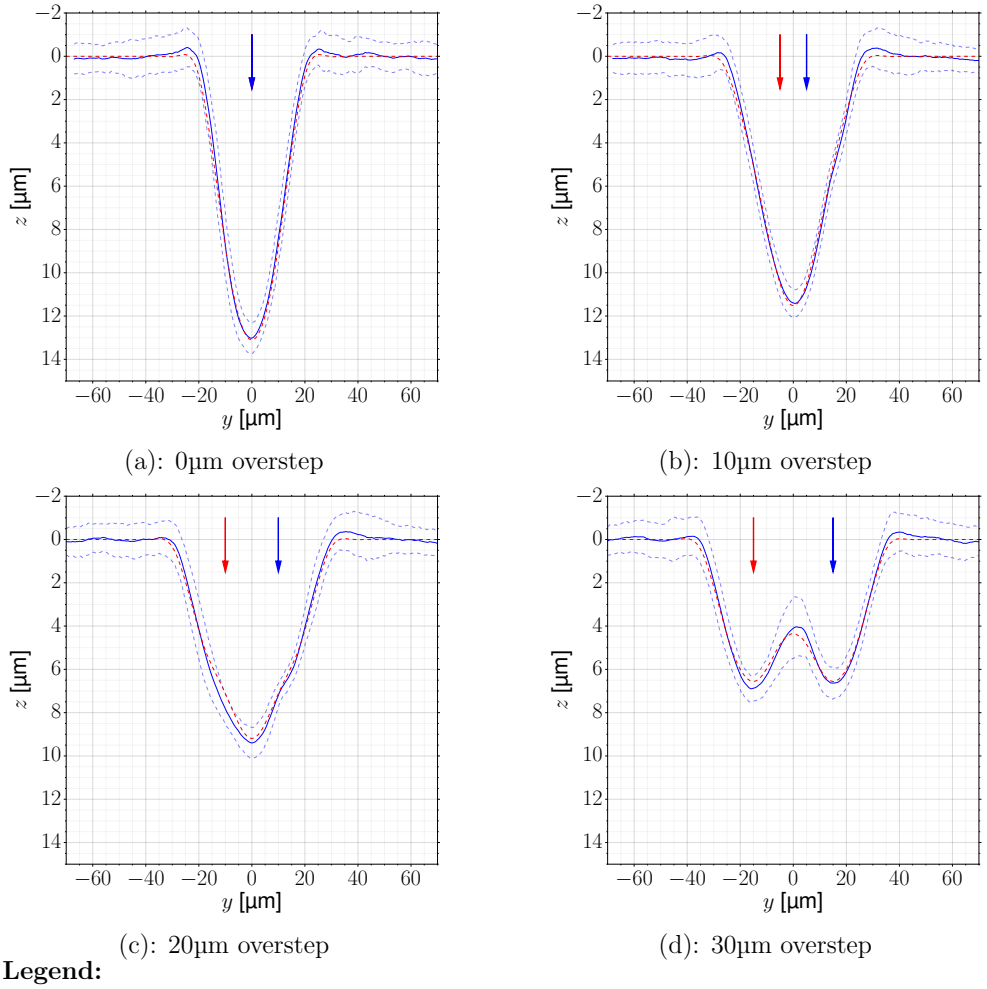

(a): 0µm overstep

(b): 10µm overstep

(c): 20µm overstep

(d): 30µm overstep

Legend:

Centre of the first trench
Centre of the second trench
Model Profile
Experimental profile
2σ variance of the experimental profile

Figure 9: Overlapping cross sections for CMX850 for trenches at 14.47W and 300 $mm.s^{-1}$ feed speed.

Table 4: Relative error in the area of the trench cross section for overlapped trenches for the three materials

		Overstep distance [µm]						
		0	10	20	30	40	50	60
		Relative Error [%]						
AF-5	18.97 W 200 mm.s^{-1}	3.78	4.15	2.77	1.58	4.56	5.89	4.73
CMX850	14.47 W 300 mm.s^{-1}	4.38	4.03	3.16	5.18	2.52	5.78	—
CMX850	18.79 W 200 mm.s^{-1}	2.68	4.83	4.91	7.87	3.02	5.14	—
Mech. PCD	18.79 W 150 mm.s^{-1}	—	3.92	9.8	6.79	7.74	4.83	—
Mech. PCD	14.47 W 300 mm.s^{-1}	9.4	9.8	7.11	6.36	5.87	1.36	—

The creation of a thin graphite layer, after the first trench is machined, dramatically changes the optical properties of the superficial layer. Thus, the graphitised layer absorbs the energy of the laser much more efficiently and therefore, it reduces the fluence necessary to ablate the surface, see Figure 10. After the first few pulses, a thin graphite layer is created and maintained by the subsequent ablation.

The model takes into account the low absorption of the first pulses and does not exhibit significant errors for single trenches. However, when mechanical PCD is the workpiece material, if the beam passes over an area already ablated, the first few pulses will be much more effective than a surface free of graphite, see Figure 11. Currently, the model does not take into

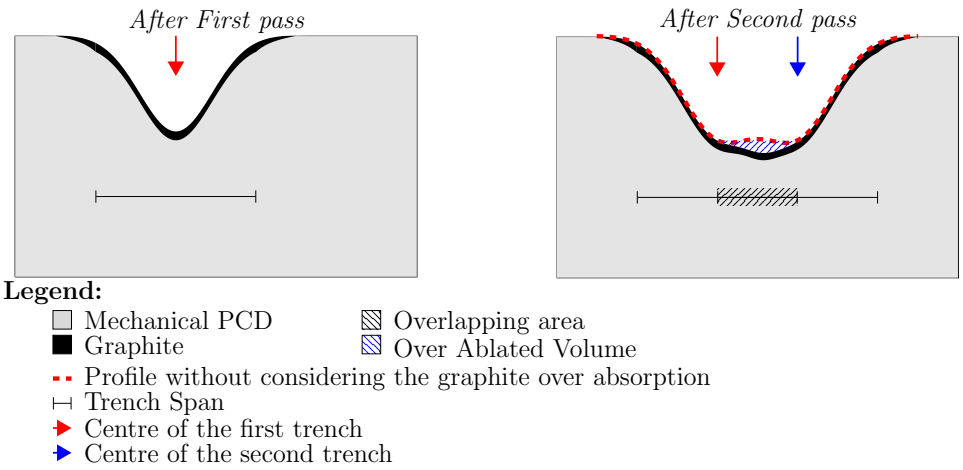

Figure 10: Scheme of the ablation pattern (creation of a small graphite layer) in the case of mechanical PCD during the overlapping of two trenches.

account changing material properties after the first pass and consequently, it under-predicts the removal of material. However, the side of the trench is accurately predicted and proves that the model is still behaving correctly outside of the affected area, see Figure 11.

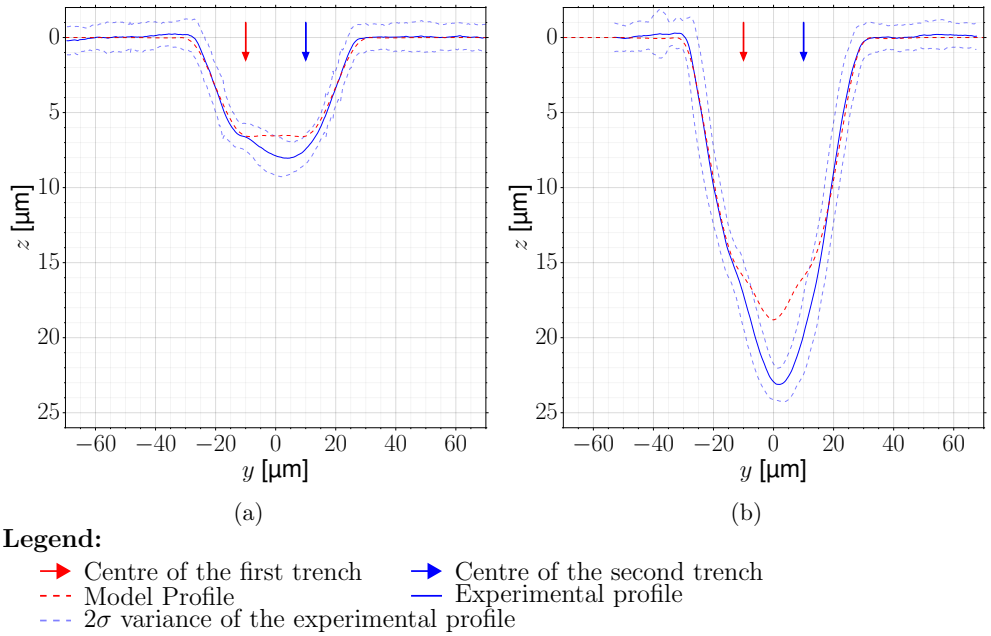

Figure 11: Overlapping test for mechanical PCD:(a) cross section at 14.47 W and 300 mm.s^{-1} with 20 µm between the centre of the two trenches. (b) cross section at 18.79 W and 150 mm.s^{-1} with 20 µm between the centre of the two trenches.

6. Conclusion

This paper has proposed and validated a new modelling framework for pulsed laser ablation. The comprehensive and innovative research approach used in this study allows the characterisation of the material removal (i.e. prediction of the single/overlapped trenches) for the pulsed laser ablation process, a crucial first step on the path to support the generation of freeform surfaces. In this respect, the main contributions of the paper are as follows:

- The model distinguishes itself by being able to be calibrated using trenches thus, contrasts with previous modelling approaches use single craters and the calibration is therefore prone to error for a few pulses, due to variability in the crater shape and depth. Furthermore, the interaction between consecutive pulses is implicitly taken into account as the proposed model uses continuous trenches for its calibration. The depth variation of the trenches with feed speed shows that consecutive pulses interact with each other and slightly enhance the ablation. This work presents conclusive evidence of the model capability to predict the shape of overlapped trenches and large scale machining of several millimetres, with average error lower than 5% for a wide range of machining conditions. Finally, the use of trenches for the model calibration leads to a simpler and more accurate calibration procedure compared to previous approaches.

- The modelling framework also highlights interesting ablation mechanisms. The evaluation of the spreading of the pulse (and a reduction of the fluence) due to the slope of the surface is a common feature added

to pulse-by-pulse previously developed models. Experimental results presented in this work show that the profile of all the trenches has the same shape for the same power (they are related by a linear function that is proportional to the dwell time at the local position). Therefore, the local slope does not seem to be important (up to a certain angle) during the ablation process. A quick calculation shows that for an angle higher than 40°, the spot spreading reduces the amount of fluence received at the local surface by around 40%. If the local angle during the ablation process is important, the trench should present a clear variation in the profile, especially for the high power and low speed. However this is not the case, therefore one can rule out a simple direct relation between the local fluence and the amount of ablated material for the tested materials. It must also be noted that the amount of ablated material during the ablation throughout the trench is not perfectly linear due to the interaction between pulses ($\beta \neq 0$). The amount of material ablated during the overlapping of trenches is linear and the local angle (up to a certain angle) does not seem to affect the amount of ablated material. It is possible to understand these results by taking into account that the evaporation of the material is a purely superficial phenomenon. Therefore, an increase in the surface area facilitates the evaporation of the material. The previous approaches (pulse-by-pulse evaluation) failed to take into account the increased surface area available for evaporation and underestimated the depth after the ablation especially for steep slopes.

- The model enables the generation of freeform features in a controlled and repeatable manner without lengthy and costly experimental trials. The model is computationally inexpensive, taking less than 10 seconds to simulate the processing of one mm^2 surface, and accurate, less than 5% error on average; it can be used as a tool to pre-compute and optimise the beam path and also as an online prediction tool in association with inline measurement systems. It represents a significant development in pulsed laser machining and allows the development of specialised CAD/CAM software for the automatic planning and optimisation of the beam path and processing parameters as presented for abrasive waterjet machining in [36].

- This modelling framework is the first step towards a numerically inexpensive generic model for pulsed laser ablation because it requires only a limited number of experimental trials to calibrate the model for any material and machining system. Furthermore, the modification of the ablation rate by various correction factors driven by experimental observations could further enhance the accuracy of the prediction and introduce the variability of the machining process [37].

The findings reported in this paper suggest that the framework can be applied to a wide range of materials. Further experimental investigations are needed to establish the capability of the model for a broader range of materials such as metals or ceramics.

Acknowledgement

This work is supported by the STEEP, Marie Curie Initial Training Network supported by the European Commission within the seventh framework program under the grant agreement n°316560.

Appendix A. Demonstration of Equation 3 and Equation 4

We wish to use Equation (1) and change the integration with respect to time to an integration with respect to the beam path arc length, s_{path} using

$$\frac{\mathrm{d}s_{\text{path}}(t)}{\mathrm{d}t} = v_{\text{feed}}. \tag{A.1}$$

where s_{path} is the equivalent arc length between the start (t_{start}) and the end (t_{end}) of the machining time defined by the path of the beam, $\underline{x}_{\text{path}}$, such that

$$s_{\text{path}} = \int_{t_{\text{start}}}^{t} \sqrt{(\partial_t x_{\text{path}})^2 + (\partial_t y_{\text{path}})^2}\mathrm{d}t. \tag{A.2}$$

Using the notation r as the distance between the centre of the beam, $\underline{x}_{\text{path}}$, and a point on the surface, $\underline{x}$,

$$r = \sqrt{(x - x_{\text{path}})^2 + (y - y_{\text{path}})^2}, \tag{A.3}$$

we find that Equation (1) is equivalent to

$$Z(x, y, P, v_{\text{feed}}) = \int_{s_{\text{start}}}^{s_{\text{end}}} \frac{E\left(P, v_{\text{feed}}, r\right)}{v_{\text{feed}}}\mathrm{d}s_{\text{path}}. \tag{A.4}$$

Since the path $\mathrm{d}s_{\text{path}}$ can be expressed as

$$\mathrm{d}s_{\text{path}} = \sqrt{1 + \left(\frac{\mathrm{d}y_{\text{path}}}{\mathrm{d}x_{\text{path}}}\right)^2}\mathrm{d}x_{\text{path}} = \mathrm{d}x_{\text{path}}, \tag{A.5}$$

because the beam is moving only in the direction x and the ablation rate is compact, Equation (3) becomes

$$v_{\text{feed}}\ Z(y, P, v_{\text{feed}}) = \int_{-\infty}^{\infty} E\left(P, v_{\text{feed}}, r\right) \mathrm{d}x_{\text{path}}. \tag{A.6}$$

Appendix B. Demonstration of the ablation rate calculation

Using the formulation of the ablation rate, Equation (9), and the standard formulation for the calculation of the surface after the ablation from the laser, Equation (1), it is possible to calculate the effect of the laser on the surface for a given power and a beam path as

$$Z(x, y) = \frac{1}{r^*} \int_{t_{\text{start}}}^{t_{\text{stop}}} [\overbrace{\alpha(P)}^{\text{Term } I} + \overbrace{\beta(P) v_{\text{feed}}(t)}^{\text{Term } II}] \bar{E}\left(\frac{r}{r^*}\right) \mathrm{d}t. \tag{B.1}$$

Using Equation (3), it is easily found that

$$II = r^* \beta \bar{p}(\bar{y}). \tag{B.2}$$

If the variation of the feed speed along the path is chosen such that

$$v_{\text{feed}}(t) = \frac{a}{b - x_{\text{path}}(t)}. \tag{B.3}$$

since the ablation rate is symmetric with respect to the y axis and defined over a compact domain,

$$I = \alpha r^* \frac{(b - x)}{a} \bar{p}(\bar{y}), \tag{B.4}$$

for x in the support of the ablation rate. Finally, the surface after the test is equal to

$$Z(x,y) = \left[\alpha\frac{(b-x)}{a} + \beta\right]\bar{p}(\bar{y}) = \left[\frac{\alpha}{v_{\text{feed}}(x)} + \beta\right]\bar{p}(\bar{y}), \tag{B.5}$$

This shows that by using the feed speed variation, Equation (B.3), along a straight path, the feature produced on the surface can be used to calibrate the whole model for a chosen power. In effect, the surface presents the exact same profile and depth that a trench machined at a constant feed speed and power should generate for a given feed speed. Therefore, it greatly reduces the number of trenches needed for an accurate calibration of the model.

References

[1] M. C. Kong, C. B. Miron, D. A. Axinte, S. Davies, and J. Kell, "On the relationship between the dynamics of the power density and workpiece surface texture in pulsed laser ablation," *CIRP Annals - Manufacturing Technology*, vol. 61, pp. 203–206, jan 2012.

[2] V. Tangwarodomnukun, P. Likhitangsuwat, O. Tevinpibanphan, and C. Dumkum, "Laser ablation of titanium alloy under a thin and flowing water layer," *International Journal of Machine Tools and Manufacture*, vol. 89, pp. 14–28, 2015.

[3] D. Dhupal, B. Doloi, and B. Bhattacharyya, "Pulsed Nd:YAG laser turning of micro-groove on aluminum oxide ceramic (Al2O3)," *International Journal of Machine Tools and Manufacture*, vol. 48, pp. 236–248, 2008.

[4] A. N. Samant and N. B. Dahotre, "Laser machining of structural ceramicsA review," *Journal of the European Ceramic Society*, vol. 29, pp. 969–993, apr 2009.

[5] P. Butler-Smith, D. Axinte, and M. Daine, "Ordered diamond micro-arrays for ultra-precision grinding – An evaluation in Ti-6Al-4V," *International Journal of Machine Tools and Manufacture*, vol. 51, pp. 54–66, jan 2011.

[6] A. K. Dubey and V. Yadava, "Laser beam machining — A review," *International Journal of Machine Tools and Manufacture*, vol. 48, pp. 609–628, may 2008.

[7] C. Dold, M. Henerichs, P. Gilgen, and K. Wegener, "Laser processing of coarse grain polycrystalline diamond (PCD) cutting tool inserts using picosecond laser pulses," *Physics Procedia*, vol. 41, pp. 610–616, 2013.

[8] C. Walter, M. Rabiey, M. Warhanek, N. Jochum, and K. Wegener, "Dressing and truing of hybrid bonded CBN grinding tools using a short-pulsed fibre laser," *CIRP Annals - Manufacturing Technology*, vol. 61, no. 1, pp. 279–282, 2012.

[9] P. Butler-Smith, D. Axinte, and M. Daine, "Solid diamond micro-grinding tools: From innovative design and fabrication to preliminary performance evaluation in Ti-6Al-4V," *International Journal of Machine Tools and Manufacture*, vol. 59, pp. 55–64, aug 2012.

[10] H. J. Booth, "Recent applications of pulsed lasers in advanced materials processing," *Thin Solid Films*, vol. 453-454, pp. 450–457, 2004.

[11] M. Pacella, P. Butler-Smith, D. A. Axinte, and M. Fay, "FIB/TEM/EELS micro/nanometric investigations of the effects of laser ablation on the diamond/binder structure in polycrystalline diamond composites," *Journal of Materials Processing Technology*, vol. 214, pp. 1153–1161, may 2014.

[12] J. Meijer, K. Du, and A. Gillner, "Laser machining by short and ultrashort pulses, state of the art and new opportunities in the age of the photons," *CIRP Annals - Manufacturing Technology*, vol. 51, no. 2, pp. 531—-550, 2002.

[13] A. V. Pakhomov, M. S. Thompson, and D. A. Gregory, "Laser-induced phase explosions in lead, tin and other elements: microsecond regime and UV-emission," *Journal of Physics D: Applied Physics*, vol. 36, pp. 2067—-2075, 2003.

[14] D. Von Der Linde and K. Sokolowski-Tinten, "The physical mechanisms of short-pulse laser ablation," *Applied Surface Science*, vol. 154–155, pp. 1–10, 2000.

[15] G. Galasso, M. Kaltenbacher, A. Tomaselli, and D. Scarpa, "A unified model to determine the energy partitioning between target and plasma in nanosecond laser ablation of silicon," *Journal of Applied Physics*, vol. 117, no. 12, p. 123101, 2015.

[16] J. Hoffman, "The effect of recoil pressure in the ablation of polycrystalline graphite by a nanosecond laser pulse," *Journal of Physics D: Applied Physics*, vol. 48, no. 23, p. 235201, 2015.

[17] P. W. Butler-Smith, D. A. Axinte, and M. Daine, "Preferentially oriented diamond micro-arrays: A laser patterning technique and preliminary evaluation of their cutting forces and wear characteristics," *International Journal of Machine Tools and Manufacture*, vol. 49, no. 15, pp. 1175–1184, 2009.

[18] K.-H. Leitz, H. Koch, A. Otto, and M. Schmidt, "Numerical simulation of process dynamics during laser beam drilling with short pulses," *Applied Physics A*, vol. 106, pp. 885–891, dec 2011.

[19] H. D. Vora, S. Santhanakrishnan, S. P. Harimkar, S. K. S. Boetcher, and N. B. Dahotre, "One-dimensional multipulse laser machining of structural alumina: evolution of surface topography," *The International Journal of Advanced Manufacturing Technology*, vol. 68, pp. 69–83, jan 2013.

[20] M. Stafe, "Theoretical photo-thermo-hydrodynamic approach to the laser ablation of metals," *Journal of Applied Physics*, vol. 112, no. 12, p. 123112, 2012.

[21] G. Pastras, A. Fysikopoulos, P. Stavropoulos, and G. Chryssolouris, "An approach to modelling evaporation pulsed laser drilling and its energy efficiency," *The International Journal of Advanced Manufacturing Technology*, vol. 72, pp. 1227–1241, 2014.

[22] P. Parandoush and A. Hossain, "A review on modelling and simulation of laser beam machining," *International Journal of Machine Tools and Manufacture*, vol. 85, pp. 135–145, 2014.

[23] B. F. Yousef, G. K. Knopf, E. V. Bordatchev, and S. K. Nikumb, "Neural network modeling and analysis of the material removal process during laser machining," *The International Journal of Advanced Manufacturing Technology*, vol. 22, pp. 41–53, sep 2003.

[24] S. Mishra and V. Yadava, "Modeling and optimization of laser beam percussion drilling of nickel-based superalloy sheet using Nd: YAG laser," *Optics and Lasers in Engineering*, vol. 51, pp. 681–695, jun 2013.

[25] A. S. Holmes, A. I. Onischenko, D. S. George, and J. E. Pedder, "Modelling of solid-state and excimer laser processes for 3D micromachining," in *SPIE Proceeding*, vol. 5713, (Williamsburg VA, USA), pp. 1–10, 2005.

[26] D. Gilbert, M. Stoesslein, D. Axinte, P. Butler-Smith, and J. Kell, "A time based method for predicting the workpiece surface micro-topography under pulsed laser ablation," *Journal of Materials Processing Technology*, vol. 214, no. 12, pp. 3077–3088, 2014.

[27] W. Hu, Y. C. Shin, and G. King, "Modeling of multi-burst mode pico-second laser ablation forimproved material removal rate," *Applied Physics A*, vol. 98, pp. 407–415, sep 2009.

[28] T. Kononenko, V. Kononenko, S. Pimenov, E. Zavedeev, V. Konov, V. Romano, and G. Dumitru, "Effects of pulse duration in laser processing of diamond-like carbon films," *Diamond and Related Materials*, vol. 14, pp. 1368–1376, aug 2005.

[29] N. H. Abel, "Auflösung einer mechanischen Aufgabe," *Journal fur die reine und angewandte Mathematik*, vol. 1, pp. 153–157, 1826.

[30] D. J. Schrock, D. Kang, T. R. Bieler, and P. Kwon, "Phase Dependent Tool Wear in Turning Ti-6Al-4V Using Polycrystalline Diamond and Carbide Inserts," *Journal of Manufacturing Science and Engineering*, vol. 136, no. 4, p. 041018, 2014.

[31] P. W. Butler-smith, D. A. Axinte, M. Pacella, and M. W. Fay, "Micro / nanometric investigations of the effects of laser ablation in the gen-

eration of micro-tools from solid CVD diamond structures," *Journal of Materials Processing Technology*, vol. 213, pp. 194–200, 2013.

[32] I. Beniaminy and M. Deutsch, "ABEL: Stable, high accuracy program for the inversion of Abel's integral equation," *Computer Physics Communications*, vol. 27, no. 4, pp. 415–422, 1982.

[33] J. Weima, A. Zaitsev, R. Job, G. Kosaca, F. Blum, G. Grabosch, W. Fahrner, and J. Knopp, "Investigation of non-diamond carbon phases and optical centers in thermochemically polished polycrystalline CVD diamond ® lms," *Journal of Solid State Electrochemistry*, vol. 4, pp. 425–434, 2000.

[34] V. I. Konov, T. V. Kononenko, and V. V. Kononenko, "Laser Micro- and Nanoprocessing of Diamond Materials," in *Optical Engineering of Diamond* (M. Rich, ed.), ch. 12, pp. 385–443, John Wiley & Sons, jan 2013.

[35] M. Seal, "Graphitization of diamond," *Nature*, vol. 185, pp. 522–523, 1960.

[36] A. Bilbao Guillerna, D. Axinte, and J. Billingham, "The linear inverse problem in energy beam processing with an application to abrasive waterjet machining," *International Journal of Machine Tools and Manufacture*, vol. 99, pp. 34–42, 2015.

[37] P. L. Torrubia, J. Billingham, and D. A. Axinte, "Stochastic simplified modelling of abrasive waterjet footprints," *Proceedings of the Royal*

Society A: Mathematical, Physical and Engineering Sciences, vol. 472, no. 20150836, 2016.